Penguin diagrams, charmless B decays, and the ''missing charm puzzle''

Alexander Lenz*
Max-Planck-Institut für Physik—Werner-Heisenberg-Institut, Föhringer Ring 6, D-80805 München, Germany

Ulrich Nierste†
DESY-Theory group, Notkestrasse 85, D-22607 Hamburg, Germany

Gaby Ostermaier‡
Physik-Department, TU München, D-85747 Garching, Germany

(Received 25 June 1997)

We calculate the contributions of penguin diagrams with internal u or c quarks to various inclusive charmless B-decay rates. Further we analyze the influence of the chromomagnetic dipole operator Q_8 on these rates. We find that the rates corresponding to $\overline{B\to X_{u\bar{u}s}}$, $\overline{B\to X_{d\bar{d}s}}$, $\overline{B\to X_{s\bar{s}s}}$, $\overline{B\to X_{s\bar{s}d}}$, and $\overline{B\to X_{d\bar{d}d}}$ are dominated by the new penguin contributions. The contributions of Q_8 sizably diminish these rates. Despite an increase of the total charmless decay rate by 36%, the new contributions are not large enough to explain the charm deficit observed by ARGUS and CLEO. We predict $n_c=1.33\pm0.06$ for the average number of charmed particles per B decay in the standard model. Then the hypothesis of an enhancement of the chromomagnetic dipole coefficient C_8 by new physics contributions is analyzed. We perform a model-independent fit of C_8 to the experimental data. If the CKM structure of the new physics contribution is the same as in the standard model, $|C_8(M_W)|$ must be enhanced by a factor of 9 to 16 in order to explain the observed charm deficit. [S0556-2821(97)07623-6]

PACS number(s): 13.20.He, 12.38.Bx, 12.39.Hg, 13.25.−k

I. INTRODUCTION

Precision measurements performed at the $\Upsilon(4S)$ resonance find less charmed particles in the final states of B meson decays than theoretically expected. The CLEO 1.5, CLEO II, and ARGUS data give [1]

$$n_c^{\rm expt}=1.15\pm0.05 \tag{1}$$

for the average number of charm (anti)quarks per B^+/B^0 decay. Complementary information on inclusive B decays can be obtained from the semileptonic branching ratio. The CLEO and ARGUS groups [1,2] have measured

$$B_{\rm SL}^{\rm expt}=10.23\pm0.39\%. \tag{2}$$

The increasing experimental precision achieved in the current decade has been paralleled by a substantial progress in the theoretical understanding of the inclusive decay rates entering $B_{\rm SL}$ and n_c. Here the calculational key is the heavy quark expansion (HQE) [3,4] of the decay rate in question: The leading term of the HQE reproduces the decay rate of a b-quark in the QCD-corrected parton model. The first nonperturbative corrections are suppressed by a factor of $(\Lambda_{\rm QCD}/m_b)^2$ and affect the rates by at most a few percent. Theoretically spectator effects of order $16\pi^2(\Lambda_{\rm QCD}/m_b)^3$ [5,6] could be larger [6], but for the decay rates of $B^\pm$ and B^0 entering Eq. (2) and Eq. (1) they are experimentally known to be at the percent level as well [7]. The apparent smallness of these nonperturbative terms has shifted the focus towards the perturbative corrections to the free quark decay. The calculation of such short distance effects starts from an effective Hamiltonian, whose generic form reads

$$H=\frac{G_F}{\sqrt{2}}\left[V_{\rm CKM}\sum_{j=1}^{2}C_jQ_j-V'_{\rm CKM}\left(\sum_{j=3}^{6}C_jQ_j+C_8Q_8\right)\right]. \tag{3}$$

Here G_F is the Fermi constant and $V_{\rm CKM}$ and $V'_{\rm CKM}$ are products of elements of the Cabibbo-Kobayashi-Maskawa (CKM) matrix. The Wilson coefficients C_j encode the physics connected to the weak scale and play the role of effective coupling constants of the local interactions described by the operators Q_j. Their precise form depends on the flavor structure of the decay and will be given below in Eq. (13).

Decays with three different flavors in the final state such as $b\to c\bar{u}d$ can only proceed through the current-current operators Q_1 and Q_2. $\Gamma(b\to c\bar{u}d)$ has been calculated to order α_s, which is the next-to-leading order (NLO), in [8]. The generic Feynman diagram for these corrections are depicted in Fig. 1. In [9] the same diagrams have been calculated for $\Gamma(b\to c\bar{c}s)+\Gamma(b\to c\bar{c}d)$. The latter decays and the charmless nonleptonic decays, however, also involve penguin effects. Diagrams with insertions of the penguin operators Q_{3-6} have been taken into account only in the leading order (LO) [10,9,11], because their coefficients C_{3-6} are much smaller than $C_{1,2}$ (cf. Table I). The results for $B_{\rm SL}$ and n_c read

$$B_{\rm SL}=(11.7\pm1.4\pm1.0)\%,\quad n_c=1.34\mp0.06. \tag{4}$$

*Electronic address: alenz@MPPMU.MPG.DE
†Electronic address: nierste@mail.desy.de
‡Electronic address: Gaby.Ostermaier@feynman.t30.physik.tu-muenchen.de

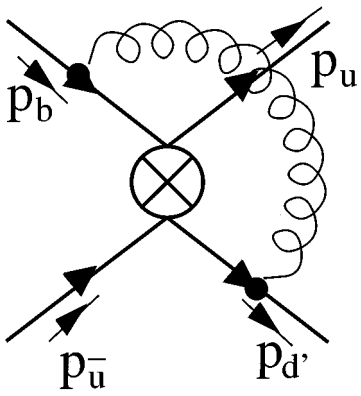

FIG. 1. Example of a current-current diagram. The cross denotes the inserted operator. d' equals d or s.

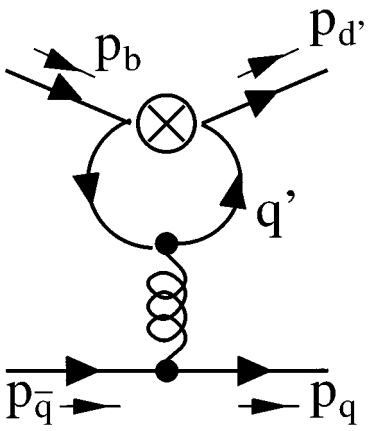

FIG. 2. Penguin diagram involving Q_2. The internal quark q' can be u or c. The corresponding diagram with Q_1 vanishes.

Here the result for $B_{\rm SL}$ has been obtained in [10,12] with the analytical input from [8,10,9]. The second error bar has been added to account for the spectator effects estimated in [6]. Apparently there is no spectacular discrepancy between Eq. (2) and Eq. (4). The result for n_c in Eq. (4) does not involve the calculation of $\Gamma(b\to c\bar{c}d)+\Gamma(b\to c\bar{c}s)$, but instead uses the experimental information on $B_{\rm SL}$ in Eq. (2) as proposed in [13,14]. We discuss this in more detail in Sec. II.

The discrepancy between Eq. (1) and Eq. (4) constitutes the ''missing charm puzzle.'' The search for a theoretical explanation has recently focused on new positive contributions to the yet unmeasured charmless decay modes entering Eq. (4). Indeed, in a recent analysis [14] $\Gamma(b\to\text{no charm})$ has been estimated indirectly in two different ways: First the experimental information on final states with hadrons containing a c quark has been used and second data on decay products involving a $\bar{c}$ quark have been analyzed. For the CLEO data both methods consistently indicate an enhancement of $\Gamma(b\to\text{no charm})$ by roughly a factor of 14 compared to the theoretical prediction in [11].

Next we briefly discuss the results from the CERN e^+e^- collider LEP for $B_{\rm SL}$ and n_c [15]. The LEP Z-peak experiments encounter a mixture of b-flavored hadrons. In order to allow for a comparison with Eq. (2), one must correct the LEP result $B_{\rm SL}^{Z,\rm expt}=10.95\pm0.42\%$ [1] for the different lifetimes [7] of the hadrons in the mixture [16]:

$$B_{\rm SL}^{Z,\rm corr,expt}=11.13\pm0.42\%,\quad n_c^{Z,\rm expt}=1.22\pm0.08. \tag{5}$$

These data are consistent with the theory [cf. Eq. (9) below], but the analysis in [14] has found evidence for an enhanced $\Gamma(b\to\text{no charm})$ also from the LEP data. Further the two methods used in [14] have given less consistent results for the LEP data than for the CLEO data. In addition the LEP measurements involve the Λ_b baryon, whose lifetime is either not properly understood theoretically or incorrectly measured. [If the latter is the case, $B_{\rm SL}^{Z,\rm corr,expt}$ in Eq. (5) must be replaced by the uncorrected $B_{\rm SL}^{Z,\rm expt}$, which reduces the 2σ discrepancy between Eq. (2) and Eq. (5).] Hence in our analysis we will mainly use Eq. (2) and Eq. (1). Now two possible sources of an enhanced $\Gamma(b\to\text{no charm})$ are currently discussed: The authors of [17] stress the possibility that the Wilson coefficient C_8 of the chromomagnetic dipole operator Q_8 is enhanced by new physics contributions. On the other hand in [14,18] an explanation within QCD dynamics is suggested: An originally produced $(c,\bar{c})$-pair can annihilate and thereby lead to a charmless final state.

The calculation of matrix elements involving Q_{3-6} and Q_8 does not exhaust all possible penguin effects. In this paper we calculate the contributions of penguin diagrams with insertions of the current-current operator Q_2 to the decay rates into charmless final states (see Fig. 2). Such a penguin

TABLE I. Wilson coefficients used in our analysis. $C_j^{(0)}$ is the LO expression, $C_j^{\rm NDR}$ is the NLO coefficient in the NDR scheme. In $C_j^{\rm NDR}$ above the NLO corrections to penguin-penguin mixing have been omitted in order to render Γ in Eq. (28) scheme independent as described in the text. For $\mu=m_b$ this affects C_3 and C_5 by 12% and 25%, but is negligible for the other coefficients. $C_j^{(0)}$ and $C_j^{\rm NDR}$ are needed for the numerical evaluation of the decay rate in Eq. (28). $\Delta\overline{C_j}$ in the last line is defined in Eq. (A1). The top and bottom mass are chosen as $m_t=m_t^{\overline{\rm MS}}(m_t)=168$ GeV and $m_b=4.8$ GeV. Further $\alpha_s(M_Z)=0.118$ [29], which corresponds to $\alpha_s(4.8\,\text{GeV})=0.216$. In the table $C_8^{(0)}=C_8^{(0),\rm eff}$ is the scheme independent coefficient mentioned in the appendix.

j	1	2	3	4	5	6	8
$C_j^{(0)}(\mu=m_b)$	−0.2493	1.1077	0.0111	−0.0256	0.0075	−0.0315	−0.1495
$C_j^{\rm NDR}(\mu=m_b)$	−0.1739	1.0731	0.0113	−0.0326	0.0110	−0.0384	
$C_j^{(0)}(\mu=m_b/2)$	−0.3611	1.1694	0.0170	−0.0359	0.0100	−0.0484	−0.1663
$C_j^{\rm NDR}(\mu=m_b/2)$	−0.2720	1.1246	0.0174	−0.0461	0.0149	−0.0587	
$C_j^{(0)}(\mu=2m_b)$	−0.1669	1.0671	0.0071	−0.0176	0.0054	−0.0202	−0.1355
$C_j^{\rm NDR}(\mu=2m_b)$	−0.1001	1.0389	0.0073	−0.0227	0.0079	−0.0251	
$\Delta\overline{C_j}(\mu=m_b)$	2.719	−1.744	0.380	−0.1050	−0.223	0.384	

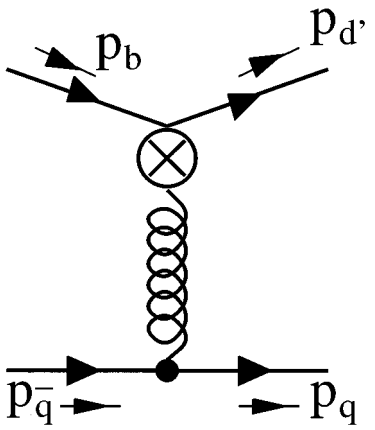

FIG. 3. Tree diagram contribution of Q_8 to $\Gamma(b\to q\overline{q}d')$.

diagram with a $(c,\overline{c})$-pair in the intermediate state involves the large coefficient C_2 and the CKM factor $V_{cb}\gg|V_{ub}|$. It is precisely the short distance analogue of the mechanism proposed in [14,18] and surprisingly has not been considered in the perturbative calculations [9–11,20] of the decay rates entering $B_{\rm SL}$ and n_c. Further we calculate the diagrams involving the interference of the tree diagram with Q_8 in Fig. 3 with Q_{1-6}, which belongs to the order α_s as well. The consideration of these diagrams is mandatory, if one wants to estimate the effect of an enhanced coefficient C_8 on $\Gamma(b\to\text{no charm})$ proposed in [17].

The paper is organized as follows: In the following section we set up our notations and collect results from earlier work. The calculation of the penguin diagram contributions and the $Q_{1-6}-Q_8$ interference terms is presented in Sec. III. The phenomenologically interested reader is referred to Sec. IV, in which we discuss our numerical results. In Sec. IV we also comment on the mechanism proposed in [18]. Further a potential enhancement of C_8 is analyzed by a model independent fit of C_8 to the experimental data. Finally we conclude.

II. PRELIMINARIES

A. $B_{\rm SL}$ and n_c

For the theoretical description of the various decay rates, it is advantageous to normalize them to the well-understood semileptonic decay rate [13,14]:

$$r_{ql}=\frac{\Gamma(\overline{B}\to X_q l\overline{\nu_l})}{\Gamma(\overline{B}\to X_c e\overline{\nu_e})},\quad r_{q_1\overline{q}_2q_3}=\frac{\Gamma(\overline{B}\to X_{q_1\overline{q}_2q_3})}{\Gamma(\overline{B}\to X_c e\overline{\nu_e})},$$

$$r_{qg}=\frac{\Gamma(\overline{B}\to X_{qg})}{\Gamma(\overline{B}\to X_c e\overline{\nu_e})},\tag{6}$$

This eliminates the factor of m_b^5 common to all decay rates. For the charmless decays we will further use

$$r_{\not c}=\sum_{\substack{q=d,s\\ q'=u,d,s}}[r_{q'\overline{q}'q}+r_{qg}]+2r_{ue}.\tag{7}$$

The semileptonic branching ratio reads

$$B_{\rm SL}=\frac{1}{2+r_{c\tau}+r_{\not c}+\Sigma_{q=d,s}(r_{c\overline{u}q}+r_{c\overline{c}q})}.\tag{8}$$

Small contributions such as $r_{u\tau}=0.004$ and radiative decay modes have been omitted in Eq. (7). In Eq. (8) also $r_{u\overline{c}s}=0.05$ [11] has been neglected. The numerical value for $B_{\rm SL}$ in Eq. (4) is the average of the two results given in [10] corresponding to two different renormalization schemes [on-shell versus modified minimal subtraction scheme ($\overline{\rm MS}$) [21] quark masses]. In the corresponding expression for n_c the term $r_{c\overline{c}s}+r_{c\overline{c}d}$, which suffers from sizable theoretical uncertainties, is eliminated in favor of $B_{\rm SL}$ [13,14]:

$$n_c=2-(2+r_{c\tau}+r_{c\overline{u}d}+r_{c\overline{u}s}+2r_{\not c})B_{\rm SL}.\tag{9}$$

Yet with [8,22]

$$r_{c\overline{u}s}+r_{c\overline{u}d}=4.0\pm0.4,\quad r_{c\tau}=0.25\tag{10}$$

and $B_{\rm SL}^{\rm exp}$ in Eq. (2) one obtains

$$n_c=1.36\mp0.04-0.205\cdot r_{\not c}.\tag{11}$$

Now the current-current type radiative corrections to $r_{\not c}$ (cf. Fig. 1) have been calculated in [20,23,8] using different renormalization schemes. The penguin operators Q_{3-6} have been included within the LO in [11]. With up-to-date values for $B_{\rm SL}$ and the CKM elements, the calculation of [11] yields $r_{\not c}=0.11\pm0.08$. Inserting this result into Eq. (11) yields the numerical value in Eq. (4). In contrast the indirect experimental determination in [14] has found $r_{\not c}=1.6\pm0.4$. In order to reproduce the experimental value of n_c in Eq. (1) one needs $r_{\not c}=1.0\pm0.4$.

So far the penguin diagrams of Fig. 2 have not been calculated for all possible charmless B decay modes. Yet for the pure penguin induced decays of a b-quark into three down-type (anti)-quarks, the contribution of the diagram of Fig. 2 has been obtained in terms of a twofold integral representation in [19]. Likewise the effect of penguin diagrams on the analysis of CP asymmetries has been studied in [19,24] and in [25] penguin effects on exclusive decays have been studied.

B. Decay rates to order α_s

In order to describe decays of the type $b\to q\overline{q}d$, one needs the following Hamiltonian:

$$H=\frac{G_F}{\sqrt{2}}\left\{\sum_{j=1}^{2}C_j(\xi_c^*Q_j^c+\xi_u^*Q_j^u)-\xi_t^*\sum_{j\in\mathcal{P}}C_jQ_j\right\},$$

$$\xi_{q'}=V_{q'b}^*V_{q'd}.\tag{12}$$

Here $\xi_u+\xi_c+\xi_t=0$ due to the unitarity of the CKM matrix

and $\mathcal{P}=\{3,\ldots,6,8\}$. H in Eq. (12) comprises the following operator basis:[1]

$$\left.\begin{aligned} Q_1^q&=(\overline{dq})_{V-A}\cdot(\overline{qb})_{V-A}\cdot\widetilde{1}\\ Q_2^q&=(\overline{dq})_{V-A}\cdot(\overline{qb})_{V-A}\cdot 1\end{aligned}\right\}\quad \text{with } q=u \text{ or } q=c,$$

$$Q_3^q=(\overline{db})_{V-A}\cdot(\overline{qq})_{V-A}\cdot 1,\quad Q_4^q=(\overline{db})_{V-A}\cdot(\overline{qq})_{V-A}\cdot\widetilde{1}$$

$$Q_5^q=(\overline{db})_{V-A}\cdot(\overline{qq})_{V+A}\cdot 1,\quad Q_6^q=(\overline{db})_{V-A}\cdot(\overline{qq})_{V+A}\cdot\widetilde{1}$$

$$Q_j=\sum_{q=u,d,s,c,b} Q_j^q \quad \text{for } 3\leqslant j\leqslant 6,$$

$$Q_8=-\frac{g}{8\pi^2}\,\overline{d}\sigma^{\mu\nu}(m_d L+m_b R)T^a b\cdot G^a_{\mu\nu}. \tag{13}$$

The color singlet and nonsinglet structure are indicated by 1 and $\widetilde{1}$ and $V\pm A$ is the Dirac structure: i.e.,

$$(\overline{dq})_{V-A}\cdot(\overline{qb})_{V-A}\cdot\widetilde{1}=\overline{d_\alpha}\gamma_\mu(1-\gamma_5)q_\beta\cdot\overline{q_\beta}\gamma^\mu(1-\gamma_5)b_\alpha.$$

Next it is useful to expand the renormalized matrix elements in α_s and to separate the result from current-current diagrams (see Fig. 1) and penguin diagrams (see Fig. 2):

$$\langle q\overline{qd}|Q_j^{q'}|b\rangle=\langle Q_j^{q'}\rangle^{(0)}+\frac{\alpha_s}{4\pi}\left(\langle Q_j^{q'}\rangle_{cc}^{(1)}+\langle Q_j^{q'}\rangle_{\text{peng}}^{(1)}\right)+O(\alpha_s^2),\quad j=1,2, \tag{14}$$

$$\langle Q_j^{q'}\rangle_{\text{peng}}^{(1)}=\sum_{k\in\mathcal{P}} r_{jk}^{q'}(p^2,m_{q'},\mu)\langle Q_k\rangle^{(0)},\quad p=p_b-p_d. \tag{15}$$

Of course $\langle Q_j^{q'}\rangle^{(0)}$ and $\langle Q_j^{q'}\rangle_{cc}^{(1)}$ are nonzero only for $q=q'=u$, recall that we do not consider $q=c$ in this work. In Eq. (15) we have expressed the result of the penguin diagram in terms of the tree-level matrix elements. There μ is the renormalization scale. For the momentum flow cf. Fig. 2.

The quark decay rate is related to the matrix element of H via

$$\Gamma(b\to q\overline{qd})=\frac{1}{2m_b}\int\frac{d^3\vec{p}_q d^3\vec{p}_{\overline{q}} d^3\vec{p}_d}{(2\pi)^5 8|E_q E_{\overline{q}} E_d|}\times\delta^{(4)}(p_b+p_{\overline{q}}-p_q-p_d)\times\overline{\langle q\overline{qd}|H|b\rangle\langle q\overline{qd}|H|b\rangle^*}.$$

The bar over $\langle q\overline{qd}|H|b\rangle\langle q\overline{qd}|H|b\rangle^*$ denotes the average over initial state polarizations and the sum over final state polarizations. Next we expand the decay rate to order α_s:

$$\Gamma(b\to q\overline{qd})=\Gamma^{(0)}+\frac{\alpha_s(\mu)}{4\pi}\left(\Delta\Gamma_{cc}+\Delta\Gamma_{\text{peng}}+\Delta\Gamma_8+\Delta\Gamma_W\right)+O(\alpha_s^2). \tag{16}$$

For $b\to q\overline{qs}$ decays one simply substitutes d by s in Eqs. (13)–(16). Now the first two terms of the NLO correction in Eq. (16) describe the effect of current-current and penguin diagrams involving Q_1 or Q_2. $\Delta\Gamma_8$ likewise contains the matrix elements of Q_8. The remaining part $\Delta\Gamma_W$ of the NLO contribution is made of the corrections to the Wilson coefficients [20,28] multiplying the tree-level amplitudes in $\Gamma^{(0)}$. We write

$$C_j(\mu)=C_j^{(0)}(\mu)+\frac{\alpha_s(\mu)}{4\pi}\,\Delta C_j(\mu),\quad j=1,\ldots 6. \tag{17}$$

Here ΔC_j is the NLO correction to the Wilson coefficient. ΔC_j depends on the renormalization scheme chosen. This scheme dependence cancels with a corresponding one in the results of the loop diagrams contained in $\Delta\Gamma_{cc}$ and $\Delta\Gamma_{\text{peng}}$. For example the scheme dependence of $\Delta C_{1,2}$ cancels in combination with the current-current type corrections to Q_1 and Q_2 of Fig. 1. Since we do not include the unknown radiative corrections to the penguin operators Q_{3-6} in Eq. (16), we must likewise leave out terms in ΔC_j related to the NLO penguin-penguin mixing in order to render Γ in Eq. (16) scheme independent. We ban these technical details into the Appendix. The values of the Wilson coefficients needed for the numerical evaluation of the various decay rates are listed in Table I.

In the LO the decays $b\to s\overline{ss}$, $b\to s\overline{sd}$, $b\to d\overline{ds}$, and $b\to d\overline{dd}$ can only proceed via Q_{3-6} and Q_8, while $b\to u\overline{ud}$ and $b\to u\overline{us}$ also receive contributions from Q_1 and Q_2. We combine both cases in

$$\Gamma^{(0)}=\frac{G_F^2 m_b^5}{64\pi^3}\left(t\sum_{i,j=1}^{2}|\xi_u|^2 C_i^{(0)}C_j^{(0)}b_{ij}+\sum_{i,j=3}^{6}|\xi_t|^2 C_i^{(0)}C_j^{(0)}b_{ij}-2t\sum_{\substack{i=1,2\\ j=3,\ldots,6}} C_i^{(0)}C_j^{(0)}\,\text{Re}(\xi_u^*\xi_t)b_{ij}\right) \tag{18}$$

with $t=1$ for $q=u$ and $t=0$ for $q=d,s$. The b_{ij}'s read

$$b_{ij}=\frac{16\pi^3}{m_b^6}\int\frac{d^3\vec{p}_q d^3\vec{p}_{\overline{q}} d^3\vec{p}_d}{(2\pi)^5 8|E_q E_{\overline{q}} E_d|}\,\delta^{(4)}(p_b+p_{\overline{q}}-p_q-p_d)\times\overline{\langle Q_i\rangle^{(0)}\langle Q_j\rangle^{(0)*}}=b_{ji} \tag{19}$$

with $Q_{1,2}=Q_{1,2}^u$ here. Setting the final state quark masses to zero, one finds

$$b_{ij}=\begin{cases}1+r/3 \text{ for } i,j\leqslant 4, \text{ and } i+j \text{ even}, & b_{55}=b_{66}=1,\\ 1/3+r \text{ for } i,j\leqslant 4, \text{ and } i+j \text{ odd}, & b_{56}=b_{65}=1/3.\end{cases} \tag{20}$$

[1]The overall sign of the matrix element $\langle Q_8\rangle$ depends on the chosen sign of the coupling g in the covariant derivative in the QCD Lagrangian. The definition in Eq. (13) complies with the result in [26,27], if the covariant derivative is chosen as $D_\mu=\partial_\mu-igT^aA_\mu^a$, so that the Feynman rule for the fermion-gluon vertex is igT^a. By convention the notation Q_7 is reserved for the magnetic $db\gamma$ operator, which we do not need in our calculation.

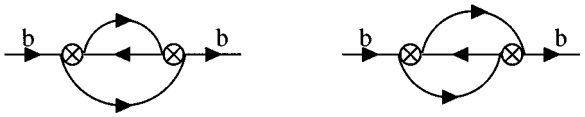

FIG. 4. The two diagrams contributing to $\Gamma^{(0)}$ in Eq. (18). The crosses represent any of Q_{1-6}.

Here $r=1$ for the decays $b\to d\overline{d}d$ and $b\to s\overline{s}s$, in which the final state contains two identical particles, and $r=0$ otherwise. The remaining b_{ij}'s are zero. Clearly for the $q\neq u$ the b_{ij}'s as defined in Eq. (19) vanish, if $i\leqslant 2$ or $j\leqslant 2$. Yet in the formulas for the decay rate, we prefer to stress this fact by keeping the parameter t, which switches the current-current effects off in the penguin induced decays. Our results in Eq. (20) agree with the zero mass limit of [10,9]. The b_{ij}'s of Eq. (19) are visualized in Fig. 4.

$\Delta\Gamma_W$ simply reads

$$\Delta\Gamma_W=\frac{G_F^2 m_b^5}{64\pi^3}2\Bigg(t\sum_{i,j=1}^{2}|\xi_u|^2[C_i^{(0)}\Delta C_j]b_{ij}+\sum_{i,j=3}^{6}|\xi_t|^2[C_i^{(0)}\Delta C_j]b_{ij}-t\sum_{\substack{i=1,2\\ j=3,\ldots,6}}[C_i^{(0)}\Delta C_j+\Delta C_i C_j^{(0)}]\mathrm{Re}(\xi_u^*\xi_t)b_{ij}\Bigg). \tag{21}$$

The current-current type corrections proportional to $C_{1,2}^{(0)}\cdot C_{1,2}^{(0)}$ are [20,23,8]

$$\Delta\Gamma_{cc}=t\,\frac{G_F^2 m_b^5}{64\pi^3}2|\xi_u|^2\sum_{i,j=1}^{2}C_i^{(0)}C_j^{(0)}h_{ij} \tag{22}$$

with t defined after Eq. (18). In the naive dimensional regularization (NDR) scheme with the standard definition of the evanescent operators [30] the diagrams of Fig. 1, the bremsstrahlung diagrams and the subsequent phase space integrations yield [8]:

$$h_{11}^{\mathrm{NDR}}=h_{22}^{\mathrm{NDR}}=\frac{31}{3}-\frac{4}{3}\pi^2,$$

$$h_{12}^{\mathrm{NDR}}\left(\frac{\mu}{m_b}\right)=h_{21}^{\mathrm{NDR}}\left(\frac{\mu}{m_b}\right)=\frac{8}{3}\ln\frac{m_b^2}{\mu^2}-\frac{17}{3}-\frac{4}{9}\pi^2 \tag{23}$$

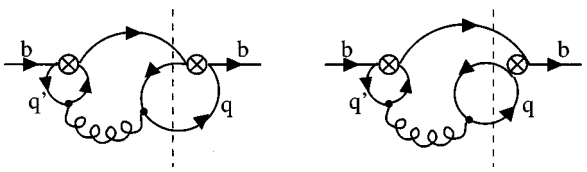

FIG. 5. The diagrams contributing to $\Delta\Gamma_{\mathrm{peng}}$ in Eq. (24). The left cross denotes $Q_1^{q'}$ or $Q_2^{q'}$ with $q'=u,c$ and the right cross represents any of Q_{1-6}. The dashed line indicates the final state with q being u, d, or s.

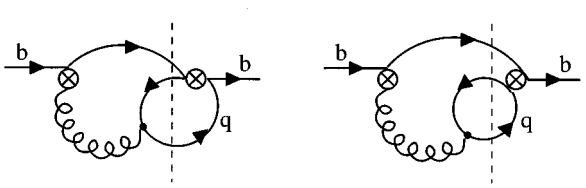

FIG. 6. The diagrams contributing to $\Delta\Gamma_8$ in Eq. (26). The left cross denotes Q_8 and the right cross represents any of Q_{1-6}.

The inclusion of $\Delta\Gamma_{cc}$ is necessary to fix the definition of the b-quark mass entering $\Gamma^{(0)}$ in Eq. (18). The values quoted in Eq. (23) correspond to the use of the (one-loop) pole quark mass in Eq. (18).

In the same way we write

$$\Delta\Gamma_{\mathrm{peng}}=\frac{G_F^2 m_b^5}{64\pi^3}2\,\mathrm{Re}\Bigg(t\sum_{i,j=1,2}C_i^{(0)}C_j^{(0)}\xi_u[\xi_c^* g_{ij}(x_c)+\xi_u^* g_{ij}(0)]-\sum_{\substack{i=1,2\\ j=3,\ldots,6}}C_i^{(0)}C_j^{(0)}\xi_t[\xi_c^* g_{ij}(x_c)+\xi_u^* g_{ij}(0)]\Bigg). \tag{24}$$

Here g_{ij} is visualized in Fig. 5 and defined by

$$g_{ij}\left(x_{q'},\frac{\mu}{m_b}\right)=\frac{16\pi^3}{m_b^6}\int\frac{d^3\vec{p}_q d^3\vec{p}_{\bar{q}} d^3\vec{p}_d}{(2\pi)^5 8|E_q E_{\bar{q}} E_d|}\times\delta^{(4)}(p_b+p_{\bar{q}}-p_q-p_d)\cdot\overline{\langle Q_i^{q'}\rangle_{\mathrm{pen}}^{(1)}\langle Q_j\rangle^{(0)*}} \tag{25}$$

with $x_{q'}=m_{q'}/m_b$. We do not display the μ dependence of the C_j's, h_{ij}'s, and g_{ij}'s in formulas for the decay rate such as Eq. (22) or Eq. (24) to simplify the notation. Now $\Delta\Gamma_{\mathrm{peng}}$ in Eq. (24) is more complicated than $\Delta\Gamma_{cc}$ in Eq. (22) for two reasons: First interference terms of different CKM structures appear and second the internal quark in the penguin graph of Fig. 2 can be $q'=c$ or $q'=u$. Further the charm quark mass enters g_{ij} with $x_c=m_c/m_b$. Finally $\Delta\Gamma_8$ in Eq. (16) is given by

$$\Delta\Gamma_8=\frac{G_F^2 m_b^5}{64\pi^3}2\,\mathrm{Re}\Bigg(-t\xi_u^*\xi_t C_8^{(0)}\sum_{j=1}^{2}C_j^{(0)}b_{j8}+|\xi_t|^2 C_8^{(0)}\sum_{j=3}^{6}C_j^{(0)}b_{j8}\Bigg). \tag{26}$$

Here the tree-level diagrams with Q_8 already contribute to order α_s.

The phase space integrations are contained in the coefficients b_{j8} in Eq. (26). They are depicted in Fig. 6 and are defined as

$$b_{j8}=\frac{16\pi^3}{m_b^6}\frac{4\pi}{\alpha_s}\int\frac{d^3\vec{p}_q d^3\vec{p}_{\bar{q}} d^3\vec{p}_d}{(2\pi)^5 8|E_q E_{\bar{q}} E_d|}\times\delta^{(4)}(p_b+p_{\bar{q}}-p_q-p_d)\overline{\langle Q_j\rangle^{(0)}\langle Q_8\rangle^{(0)*}}=b_{8j}. \quad (27)$$

It is instructive to insert the above expressions for $\Delta\Gamma_{cc}$, $\Delta\Gamma_{\rm peng}$, and $\Delta\Gamma_8$ into Eq. (16). The decay rate then reads

$$\Gamma=\frac{G_F^2 m_b^5}{64\pi^3}\,\mathrm{Re}\Bigg[t\sum_{i,j=1}^{2}C_iC_j\Bigg(|\xi_u|^2 b_{ij}+\frac{\alpha_s(\mu)}{4\pi}|\xi_u|^2\times 2[h_{ij}+g_{ij}(0)-g_{ij}(x_c)]-\frac{\alpha_s(\mu)}{4\pi}\,\xi_u\xi_t^*\,2g_{ij}(x_c)\Bigg)-2\sum_{\substack{i=1,2\\ j=3,\dots 6}}C_iC_j\Bigg(t\xi_u^*\xi_t b_{ij}+\frac{\alpha_s(\mu)}{4\pi}\times\xi_u^*\xi_t[g_{ij}(0)-g_{ij}(x_c)]-\frac{\alpha_s(\mu)}{4\pi}\,|\xi_t|^2 g_{ij}(x_c)\Bigg)+\sum_{i,j=3}^{6}C_iC_j|\xi_t|^2 b_{ij}+\frac{\alpha_s(\mu)}{4\pi}\times C_8\Bigg(-t\xi_u^*\xi_t\sum_{j=1}^{2}C_j 2b_{j8}+|\xi_t|^2\sum_{j=3}^{6}C_j 2b_{j8}\Bigg)\Bigg]. \quad (28)$$

Here the C_j's are the Wilson coefficients of Eq. (17) including NLO corrections. $C_j^{(0)}$ rather than $C_j^{\rm NDR}$ should be used in the terms of order α_s in Eq. (28) for consistency. The unitarity of the CKM matrix has been used to eliminate ξ_c from Eq. (28).

From Eq. (24) or Eq. (28) one notices that penguin induced decays with $t=0$ receive radiative corrections proportional to the large coefficient C_2, which does not enter the tree-level decay rate in Eq. (18). Further $\Delta\Gamma_{\rm peng}$ depends on the CKM phase δ, because ξ_u, ξ_t, and the loop functions g_{ij} are complex. Decay rates and CP asymmetries for these penguin induced decays have been derived in [19] in terms of a twofold integral representation taking into account the interference of the penguin diagram involving Q_2 with Q_{1-6}. In Sec. III we derive analytical results for the decay rates and also include $\Delta\Gamma_8$.

In the decays $b\to u\bar{u}d$ and $b\to u\bar{u}s$, the main focus is on the first sum in $\Delta\Gamma_{\rm peng}$ in Eq. (24) containing products of two of the large coefficients C_1 and C_2. We also keep the second sum in Eq. (24), but remark here that these terms are not the full set of one-loop radiative corrections involving one large coefficient $C_{1,2}$ and one small coefficient C_{3-6}: In addition to the radiative corrections calculated in this paper, there are also current-current diagrams (see Fig. 1) and penguin diagrams (see Fig. 2) with penguin operators Q_{3-6}. In decays with a $(u,\bar{u})$-pair in the final state, these matrix elements interfere with those of Q_1^u and Q_2^u and therefore also yield a term proportional to $C_{1,2}\cdot C_{3-6}$.

The terms proportional to $C_j\cdot C_8$ comprised in $\Delta\Gamma_8$ are interesting in order to confirm or falsify the mechanism proposed in [17]. If new physics indeed dominates C_8, then $\Gamma(b\to s+g)\propto|C_8|^2$ considered in [17] is enhanced. Yet $\Delta\Gamma_8$ is linear in C_8, so that the sign of the new physics contribution may determine whether $\Gamma(b\to$no charm$)$ is enhanced or diminished. A calculation similar to ours has been partly done in [31]. Yet in [31] some questionable approximations have been made: For example the operator mixing has been neglected and the top quark has not been integrated out, but instead formally treated as a light particle. In some cases the results of [31] differ substantially from those in [19].

We close this section with the formula relating Γ in Eq. (28) to the $r_{q_1\bar{q}_2 q_3}$'s defined in Eq. (6). To this end we need the semileptonic decay rate to order α_s [32]:

$$\Gamma(b\to ce\overline{\nu_e})=\frac{G_F^2 m_b^5}{192\pi^3}\,|V_{cb}|^2 f_1(x_c^2)\Bigg(1+\frac{\alpha_s(\mu)}{2\pi}\,h_{\rm SL}(x_c)+O(\alpha_s^2)\Bigg).$$

The tree-level phase space function is

$$f_1(a)=1-8a-12a^2\ln a+8a^3-a^4.$$

The analytic expression for $h_{\rm SL}(x_c)$ can be found in [8,32]. The approximation

$$h_{\rm SL}(x_c)=-3.341+4.05(x_c-0.3)-4.3(x_c-0.3)^2$$

holds to an accuracy of 1 permille in the range $0.2\leqslant x_c\leqslant 0.4$. Here $x_c=m_c/m_b$ is the ratio of the one-loop pole masses. We further include the hadronic corrections to the free quark decay of order $1/m_b^2$ obtained from the HQE [3]. This yields

$$r_{q\bar{q}\bar{d}}=\frac{192\pi^3}{G_F^2 m_b^5|V_{cb}|^2 f_1(x_c^2)}\Bigg\{\Gamma+\Gamma^{(0)}\Bigg[6\Bigg(\frac{(1-x_c^2)^4}{f_1(x_c^2)}-1\Bigg)\frac{\lambda_2}{m_b^2}-\frac{\alpha_s(\mu)}{2\pi}\,h_{\rm SL}(x_c)\Bigg]+\delta\Gamma\Bigg\}. \quad (29)$$

Here $\lambda_2=0.12\ \mathrm{GeV}^2$ encodes the chromomagnetic interaction of the b-quark with the light degrees of freedom. Further corrections are contained in $\delta\Gamma$. It is obtained from $\Gamma^{(0)}$ by substituting b_{ij} with δb_{ij} in the definition (18). One finds, from [3],

$$\delta b_{12}=\delta b_{14}=\delta b_{21}=\delta b_{23}=\delta b_{32}=\delta b_{34}=\delta b_{41}=\delta b_{43}=-8\frac{\lambda_2}{m_b^2}=-0.042\quad\text{for } m_b=4.8\ \mathrm{GeV},$$

while $\delta b_{56}=\delta b_{65}$ is unknown yet. If there are no identical quarks in the final state, the remaining δb_{ij}'s vanish. Otherwise

$$\delta b_{33}=\delta b_{44}=\delta b_{34},\quad \delta b_{55}=\delta b_{66}\neq 0\quad\text{for } b\to d\bar{d}d \text{ and } b\to s\bar{s}s \quad (30)$$

with δb_{66} unknown. The dependence on λ_1 parametrizing the effect of the b-quark's Fermi motion on the decay rates cancels in the ratio in Eq. (29).

For the calculation of r_ℓ in Eq. (7) we also need r_{ue} and r_{sg}. The corresponding expressions are [3,27]

$$r_{ue}=\left|\frac{V_{ub}}{V_{cb}}\right|^2 \frac{1}{f_1(x_c^2)}\left[1+\frac{\alpha_s(\mu)}{2\pi}\left[h_{\rm SL}(0)-h_{\rm SL}(x_c)\right]+6\left(\frac{(1-x_c^2)^4}{f_1(x_c^2)}-1\right)\frac{\lambda_2}{m_b^2}\right],$$

$$r_{sg}=\left|\frac{V_{tb}^* V_{ts}}{V_{cb}}\right|^2 \frac{8\alpha_s(\mu)}{\pi f_1(x_c^2)}\left[C_8(\mu)\right]^2.$$

III. CALCULATION

This section is devoted to the calculation of the g_{ij}'s and b_{j8}'s entering Eqs. (24), (26), (28). All results correspond to the NDR scheme. The first step is the same for all b decays under consideration: The penguin diagram of Fig. 2 must be calculated to obtain the r_{ij}'s in Eq. (15):

$$r_{24}(p^2,m,\mu)=\frac{1}{3}\log\frac{m^2}{\mu^2}-\frac{2}{9}-\frac{4m^2}{3p^2}-\frac{1}{3}\left(1+\frac{2m^2}{p^2}\right)\sqrt{1-4m^2/p^2+i\delta}\,\log\frac{\sqrt{1-4m^2/p^2+i\delta}-1}{\sqrt{1-4m^2/p^2+i\delta}+1},$$

$$r_{24}(p^2,0,\mu)=\frac{1}{3}\left(\log\frac{p^2}{\mu^2}-i\pi\right)-\frac{2}{9}, \tag{31}$$

$$r_{26}=r_{24},\quad r_{23}=r_{25}=-\tfrac{1}{3}r_{24}. \tag{32}$$

Here $p=p_b-p_d$ is the momentum flowing through the gluon leg and m is the internal quark mass. The infinitesimal ''$i\delta$''-prescription yields the correct sign of the imaginary part of the logarithm in the case $p^2>4m^2$ and likewise regulates the square root for $p^2<4m^2$. The r_{1j}'s and r_{28} are zero.

Next we combine Eq. (25) and Eq. (15) to obtain the coefficients g_{ij} in Eq. (24) and Eq. (28):

$$g_{ij}\left(x_c,\frac{\mu}{m_b}\right)=\frac{16\pi^3}{m_b^6}\int\frac{d^3\vec{p}_q d^3\vec{p}_{\bar{q}} d^3\vec{p}_d}{(2\pi)^5 8|E_q E_{\bar{q}} E_d|}\,\delta^{(4)}(p_b+p_{\bar{q}}-p_q-p_d)\cdot\sum_{k=1}^{6} r_{ik}^c[(p_b-p_d)^2,x_c m_b,\mu]\times\overline{\langle Q_k\rangle^{(0)}\langle Q_j\rangle^{(0)*}}. \tag{33}$$

The corresponding expression for an internal u-quark is obtained by substituting c with u in Eq. (33). For the decays $b\to u\bar{u}d$, $b\to u\bar{u}s$, $b\to s\bar{s}d$, and $b\to dds$ one finds

$$g_{22}\left(x_c,\frac{\mu}{m_b}\right)=g_{24}\left(x_c,\frac{\mu}{m_b}\right)=g_{26}\left(x_c,\frac{\mu}{m_b}\right)=\frac{16}{27}\ln\frac{x_c m_b}{\mu}-\frac{16}{27}(1-10x_c^2+18x_c^4-36x_c^6)\times\sqrt{1-4x_c^2}\,\ln\frac{1-\sqrt{1-4x_c^2}}{2x_c}+\frac{4}{9}\left[-\frac{3}{2}+16x_c^2-14x_c^4+24x_c^6+32x_c^6(2-3x_c^2)\left(\ln^2\frac{1-\sqrt{1-4x_c^2}}{2x_c}-\frac{\pi^2}{4}\right)\right]$$

$$-i\pi\frac{4}{9}\left[\frac{2}{3}\sqrt{1-4x_c^2}(1-10x_c^2+18x_c^4-36x_c^6)-32x_c^6(2-3x_c^2)\ln\frac{1-\sqrt{1-4x_c^2}}{2x_c}\right]$$

$$g_{22}\left(0,\frac{\mu}{m_b}\right)=g_{24}\left(0,\frac{\mu}{m_b}\right)=g_{26}\left(0,\frac{\mu}{m_b}\right)=\frac{4}{9}\left(-\frac{3}{2}+\frac{4}{3}\ln\frac{m_b}{\mu}-\frac{2}{3}i\pi\right)$$

$$g_{21}\left(x,\frac{\mu}{m_b}\right)=g_{23}\left(x,\frac{\mu}{m_b}\right)=g_{25}\left(x,\frac{\mu}{m_b}\right)=g_{1j}\left(x,\frac{\mu}{m_b}\right)=0,\quad j=1,\ldots,6, \tag{34}$$

where $x_c=m_c/m_b$. Numerically one finds, for actual quark masses,

$$g_{22}(0,1)=-0.67-0.93i,\quad g_{22}(0.3,1)=-0.69-0.23i. \tag{35}$$

The near equality of the real parts in Eq. (35) is a numerical accident.

In the case of two identical particles in the final state, both diagrams of Fig. 5 contribute. Then g_{23} is no more zero, but

$$g_{23}\left(x,\frac{\mu}{m_b}\right)=g_{22}\left(x,\frac{\mu}{m_b}\right)\quad\text{for } b\to d\bar{d}d \text{ and } b\to s\bar{s}s. \tag{36}$$

The remaining g_{ij}'s are as in Eq. (34). As an analytical check we have confirmed that the μ-dependence in Eq. (34) and Eq. (36) cancels with the μ-dependence in the Wilson coefficients in Eq. (18) to order α_s.

We now turn to the calculation of $\Delta\Gamma_8$ in Eq. (26). Performing the phase space integration in Eq. (27) yields

TABLE II. The values of $r_{q\bar{q}q'}$ for the various final states as defined in Eq. (6). The input parameters are chosen as in Eq. (39) except for the quantity listed in the second column. The last column lists r_ϕ defined in Eq. (7). B in the last row is the branching ratio for $B\to X_{q\bar{q}q'}$, obtained by multiplying $r_{q\bar{q}q'}$ with $B_{\rm SL}=10.23\%$.

		Final state						
	Input	$u\bar{u}d$	$u\bar{u}s$	$d\bar{d}s$	$s\bar{s}s$	$s\bar{s}d$	$d\bar{d}d$	No charm
$r_{q\bar{q}q'}$	as in Eq. (39)	0.040	0.021	0.018	0.015	8.9×10^{-4}	7.2×10^{-4}	0.14
	$\mu=m_b/2$	0.044	0.033	0.029	0.024	14.0×10^{-4}	11.4×10^{-4}	0.19
	$\mu=2m_b$	0.037	0.014	0.011	0.009	5.5×10^{-4}	4.6×10^{-4}	0.11
	$\left\|\frac{V_{ub}}{V_{cb}}\right\|=0.06$	0.023	0.020	0.018	0.015	8.7×10^{-4}	7.1×10^{-4}	0.11
	$\left\|\frac{V_{ub}}{V_{cb}}\right\|=0.10$	0.062	0.023	0.018	0.015	9.1×10^{-4}	7.5×10^{-4}	0.18
	$\delta=60°$	0.044	0.017	0.018	0.015	5.9×10^{-4}	4.8×10^{-4}	0.14
	$\delta=120°$	0.036	0.025	0.018	0.014	12.2×10^{-4}	10.0×10^{-4}	0.14
	$x_c=0.25$	0.034	0.019	0.016	0.013	8.1×10^{-4}	6.7×10^{-4}	0.12
	$x_c=0.33$	0.048	0.023	0.020	0.017	9.7×10^{-4}	7.9×10^{-4}	0.16
B	as in Eq. (39)	0.41%	0.22%	0.18%	0.15%	9.1×10^{-3}%	7.4×10^{-3}%	1.4%

$$b_{28}=b_{48}=b_{68}=-\tfrac{16}{9},$$

$$b_{18}=b_{38}=b_{58}=0 \tag{37}$$

for $b\to u\bar{u}d$, $b\to u\bar{u}s$, $b\to s\bar{s}d$, and $b\to d\bar{d}s$. If identical particles are present, b_{38} is no more zero, but instead reads

$$b_{38}=-\frac{16}{9} \quad \text{for } b\to d\bar{d}d \text{ and } b\to s\bar{s}s. \tag{38}$$

The remaining b_{j8}'s are as in Eq. (37).

IV. CHARMLESS DECAY RATES

A. Standard model

In this section we discuss our numerical results for the various decay rates. We use the following set of input parameters:

$$\left|\frac{V_{ub}}{V_{cb}}\right|=0.08\pm0.02,\ \ \delta=90°\pm30°,\ \ x_c=0.29\pm0.04,$$

$$\mu=m_b=4.8\ \text{GeV},$$

$$\alpha_s(M_Z)=0.118,\ \ |V_{cb}|=0.038,\ \ m_t(m_t)=168\ \text{GeV}. \tag{39}$$

The $r_{q\bar{q}q'}$'s sizably depend on $|V_{ub}/V_{cb}|$, δ, x_c and especially on the renormalization scale, which will be varied in the range $m_b/2\leq\mu\leq2m_b$. The quark masses in Eq. (39) are taken from [33], the values for $|V_{ub}/V_{cb}|$ and $|V_{cb}|$ have been presented in [34]. The range for the CKM phase δ has been obtained from the NLO analysis of ϵ_K and Δm_B in [35]. The dependence on $\alpha_s(M_Z)$ in the range $0.112\leq\alpha_s(M_Z)\leq0.124$ [29] is weaker than the μ-dependence. Our results are listed in Table II.

Keeping the physical input parameters as in Eq. (39) and varying the scale in the range $m_b/2\leq\mu\leq2m_b$, the charmless decay modes sum to

$$r_\phi=0.15\pm0.04.$$

The values for r_{sg} and r_{ue} entering this result are

$$r_{sg}=0.02\pm0.01,\quad r_{ue}=0.01\pm0.00.$$

Incorporating also the uncertainties in $|V_{ub}/V_{cb}|$ and x_c, one finds

$$r_\phi=0.15\pm0.08. \tag{40}$$

To discuss the results for the individual charmless decay modes, it is instructive to look at the separate scheme-independent contributions from $\Gamma^{(0)}$, $\Delta\overline{\Gamma}_{cc}$, $\Delta\overline{\Gamma}_{\rm peng}$, $\Delta\overline{\Gamma}_8$, and $\Delta\overline{\Gamma}_W$ (cf. the Appendix) to the decay rate. These contributions are listed in Table III, in which also the contributions from penguin operators to $\Gamma^{(0)}$ are shown.

All decays except for $B\to X_{u\bar{u}d}$ are dominated by penguin effects. The sizable μ-dependence in these decays can be reduced by calculating the current-current type radiative corrections to penguin operators. Note that all these decay rates are even dominated by the penguin diagrams calculated in this work. On the other hand the terms stemming from Q_8 lower the penguin induced rates. In $B\to$no charm, however, the net effect of Q_8 is positive because of the two-body decay $b\to sg$ proportional to C_8^2.

The calculation of r_ϕ in [11] has included $\Gamma^{(0)}$, $\Delta\overline{\Gamma}_W$, and $\Delta\overline{\Gamma}_{cc}$. Taking into account that in [11] a high (theoretical) value for $B_{\rm SL}$ has been used, the result of [11] translates into

$$r_\phi=0.04 \ \text{ for } \left|\frac{V_{ub}}{V_{cb}}\right|=0.10.$$

The corresponding value in Table II is $r_\phi=0.18$ showing the increase due to $\Delta\overline{\Gamma}_{\rm peng}+\Delta\overline{\Gamma}_8$. Despite the 36% increase in r_ϕ in Eq. (40), the value is still much below $r_\phi=1.0\pm0.4$ needed to solve the missing charm puzzle. The new theoretical prediction for n_c is

$$n_c=1.33\mp0.06,$$

TABLE III. Separate contributions to $\Gamma(b\to q\bar{q}q')$ in percent of the total rate for the input parameters of Eq. (39). In the third column the contribution from the LO matrix elements of penguin operators and their interference with matrix elements of $Q_{1,2}$ is shown. In the last row $\Gamma(b\to ue\bar{\nu}_e)$ entering $r_{\not c}$ has been assigned to the second column listing the current-current part.

Final state	$\propto C_{1,2}^{(0)}\cdot C_{1,2}^{(0)}$	$\propto C_{3-6}^{(0)}\cdot C_{1-6}^{(0)}$	$\propto\Delta\overline{\Gamma}_W$	$\propto\Delta\overline{\Gamma}_{cc}$	$\propto\Delta\overline{\Gamma}_{\text{peng}}$	$\propto\Delta\overline{\Gamma}_8$
$u\bar{u}d$	107	−4	−5	6	−5	1
$u\bar{u}s$	10	39	−7	1	72	−14
$d\bar{d}s$	0	46	−8	0	78	−16
$s\bar{s}s$	0	44	−20	0	92	−16
$s\bar{s}d$	0	54	−9	0	74	−19
$d\bar{d}d$	0	52	−24	0	91	−19
sg	0	0	0	0	0	100
No charm	46	17	−6	2	31	11

which is only marginally lower than the old result in Eq. (4). Still an enhancement of $r_{\not c}$ by a factor between 2.6 and 20 is required. Yet with the result in Eq. (34) for the penguin diagram of Fig. 5 at hand, we can estimate the nonperturbative enhancement of the $(c,\bar{c})$ intermediate state necessary to reproduce the experimental result. The mechanism proposed in [14,18] corresponds to a violation of quark-hadron duality, which we may parametrize by multiplying the $(c,\bar{c})$-penguin function $g_{ij}(x_c,\mu/m_b)$ in Eq. (28) by an arbitrary factor d. We find that d must be chosen as large as 20 in order to reach the lowest desired value $r_{\not c}=0.6$ for the central set of the input parameters in Eq. (39). Yet in this case one must also include the double-penguin diagram obtained by squaring the result of Fig. 2. Taking this into account, nonperturbative effects must still increase the $(c,\bar{c})$-penguin diagram by roughly a factor of 9 over its short distance result in the NDR scheme. Having in mind that the phase space integration contained in $g_{ij}(x_c,\mu/m_b)$ implies a smearing of the invariant hadronic mass of the $(c,\bar{c})$-pair, such a large deviation of quark-hadron duality seems unlikely.

Our results for the branching fractions of $b\to d\bar{d}s$ and $b\to s\bar{s}s$ differ by roughly a factor of 1/2 from the results in [19]. The main source of the discrepancy is the different calculation of the total rate Γ_{tot} entering the theoretical definition of the branching fraction. Our predictions for the branching ratios in Table II contain the total rate via $\Gamma_{\text{tot}}=\Gamma_{\text{SL}}/B_{\text{SL}}^{\text{exp}}$, while in [19] $\Gamma_{\text{tot}}=G_F^2m_b^5|V_{cb}|^2/(64\pi^3)$ has been used. This approximation neglecting the RG effects appears to be too crude and is responsible for 50% of the discrepancy. The remaining difference is due to the effect of $\Delta\Gamma_8$ not considered in [19] and the use of different values of the Wilson coefficients. Our predictions for $B(b\to s\bar{s}d)$ and $B(b\to ddd)$ are even smaller by a factor of 5 than the results of [19]. This is due to the fact that in addition the value of $|V_{td}/V_{cb}|^2$ used in [19] is more than twice as large as the present day value used in our analysis. We remark that with our new results the number of B-mesons to be produced in order to detect the inclusive CP asymmetries corresponding to these decays is substantially larger than estimated in [19].

B. New physics

In the standard model the initial conditions for C_{3-6} and C_8 are generated at a scale $\mu=O(M_W)$ by the one-loop bsg-vertex function with a W-boson and a top quark as internal particles. Because of the helicity structure of the couplings positive powers of m_t are absent in the bsg-vertex. In many extensions of the standard model such a helicity suppression does not occur [17]. Further in supersymmetric extensions flavor changing transitions can be mediated by gluinos, whose coupling to (s) quarks involves the strong rather the weak coupling constant. Recently a possible enhancement of C_8 affecting r_{sg} and thereby $r_{\not c}$ has attracted much attention [17]. In the following we will perform a model independent analysis of this hypothesis.

New physics affects the initial condition of the Wilson coefficients calculated at the scale of the masses mediating the flavor-changing transition of interest. We will take $\mu=M_W$ as the initial scale for both the standard and nonstandard contributions to the Wilson coefficients. The renormalization group evolution down to $\mu=m_b$ mixes the various initial values and can damp or enhance the new physics effects in $C_i(M_W)$. For example the standard model value of

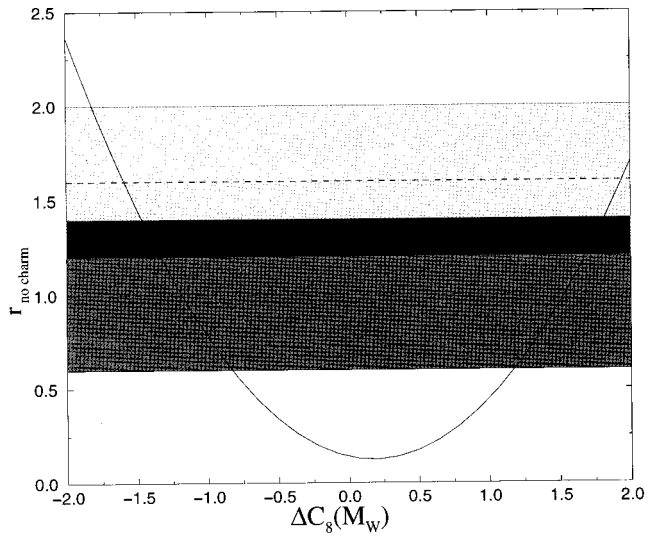

FIG. 7. $r_{\not c}$ vs $\Delta C_8(M_W)$ parametrizing new physics contributions to $C_8(M_W)$. The dark shading marks the region $r_{\not c}=1.0\pm0.4$ needed to reproduce the experimental result for n_c in Eq. (1). The lightly shaded area corresponds to $r_{\not c}=1.6\pm0.4$ obtained from the analysis in [14].

C_8 (4.8 GeV) in Table I is mainly a linear combination of $C_2(M_W)$ and $C_8(M_W)$:

$$C_8(m_b) = -0.08 C_2(M_W) + 0.7 C_8(M_W)$$

with $C_8(M_W) = -0.1$. If one enlarges $C_8(M_W)$ by a factor of 10 while keeping $C_{1-6}(M_W)$ fixed, $r_{\not c}$ grows by a factor of 5.5. The sensitivity of $r_{\not c}$ to $C_{3-6}(M_W)$ is much smaller, increasing the latter by a factor of 10 enhances $r_{\not c}$ only by a factor of 1.6. Hence in the following we will only focus on $C_8(M_W) = -0.1 + \Delta C_8(M_W)$, where $\Delta C_8(M_W)$ is the new physics contribution. For simplicity we will further assume that the CKM structure of the new contributions is the same as in the standard model and neglect the possibility of new CP-violating phases by assuming $\Delta C_8(M_W)$ to be real.

In Fig. 7 $r_{\not c}$ is plotted versus $\Delta C_8(M_W)$. Solving for $r_{\not c} = 1.0 \pm 0.4$ yields two solutions:

$$\Delta C_8(M_W) = -1.2^{-0.3}_{+0.4}, \quad \Delta C_8(M_W) = 1.5 \pm 0.3. \quad (41)$$

The central values correspond to an enhancement of the standard model value for $C_8(M_W)$ by factors of 13 and (-14). We hope to resolve the twofold ambiguity after calculating the contribution of Q_8 to $\Gamma(\overline{B} \to X_{c\bar{c}s})$.

The LEP data in Eq. (5) correspond to $r_{\not c} = 0.4 \pm 0.5$ and

$$\Delta C_8(M_W) = -0.5^{-0.6}_{+0.5}, \quad \Delta C_8(M_W) = 0.9^{+0.6}_{-0.9}$$

showing the consistency of Eq. (5) with the standard model.

V. CONCLUSIONS

We have calculated two new contributions to the inclusive decay rates of B-mesons into various charmless final states: First we have obtained the results of penguin diagrams involving the operator Q_2 and a c- or u-quark in the loop putting special care on the renormalization scheme independence of our results. Second we have calculated the influence of the chromomagnetic dipole operator Q_8 on these decays. The former contributions have been found to dominate the branching fractions for $\overline{B} \to X_{u\bar{u}s}$, $\overline{B} \to X_{d\bar{d}s}$, $\overline{B} \to X_{s\bar{s}s}$, $\overline{B} \to X_{s\bar{s}d}$, and $\overline{B} \to X_{d\bar{d}d}$. The effect of Q_8 on these decay modes is also sizable and decreases the rates. On the other hand the decay rate for $\overline{B} \to X_{u\bar{u}d}$ is only affected by a few percent. Our results increase the theoretical prediction for $B(\overline{B} \to \text{no charm})$ by 36%, which is not sufficient to explain the charm deficit observed in B-decays by ARGUS and CLEO. If a breakdown of quark-hadron duality due to intermediate $(c,\bar{c})$ resonances is to explain the ''missing charm puzzle,'' the phase space integrated penguin diagram with an internal c-quark must be larger than the perturbative result in the NDR scheme by roughly a factor of 9.

We have then analyzed the hypothesis that new physics effects enhance the coefficient C_8 of Q_8 and have performed a model independent fit of C_8 to the experimental data on n_c. The renormalization group evolution from $\mu = M_W$ to $\mu = m_b$ has been properly taken into account. One finds two solutions for C_8: For the central values of the theoretical input and the data of the $\Upsilon(4S)$ experiments $C_8(M_W)$ must be larger by a factor of 13 or (-14) than in the standard model, if the new physics contributions have the same CKM structure as the standard model penguin diagram.

ACKNOWLEDGMENTS

We are grateful to Andrzej Buras for many stimulating discussions. U.N. acknowledges interesting discussions with Stefano Bertolini, *Christoph Greub, Antonio Masiero, and Yong-Yeon Keum. This work was supported by BMBF under Contract No. 06-TM-874.

APPENDIX: SCHEME INDEPENDENCE

Now we discuss the cancellation of scheme dependent terms between the NLO Wilson coefficients and the loop diagrams contained in $\Delta\Gamma_{cc}$ and $\Delta\Gamma_{\text{peng}}$. We define scheme independent combinations $\Delta\overline{\Gamma}_{cc}$, $\Delta\overline{\Gamma}_{\text{peng}}$, and $\Delta\overline{\Gamma}_W$, which allow a meaningful discussion of the numerical sizes of these separate contributions to Γ as performed in Sec. IV. Finally we comment on the scheme independence of $\Delta\Gamma_8$.

The NLO correction to the Wilson coefficients in Eq. (17) can be split into two parts:

$$\Delta C_j(\mu) = \sum_{k=1}^{6} J_{jk} C_k^{(0)}(\mu) + \Delta\overline{C}_j(\mu), \quad j = 1, \ldots, 6. \quad (A1)$$

$\Delta\overline{C}_j(\mu)$ contains the contributions stemming from the weak scale. It is independent of the renormalization scheme and proportional to $\alpha_s(M_W)/\alpha_s(\mu)$. Yet the J_{jk}'s in Eq. (A1) are scheme dependent. The precise definitions of the terms in Eq. (A1) can be found in [28,30]. We now absorb the terms involving J_{jk} into $\Delta\overline{\Gamma}_{cc}$ and $\Delta\overline{\Gamma}_{\text{peng}}$, so that the latter become scheme independent.

The identification of scheme independent combinations of one-loop matrix elements and J_{jk}'s is most easily done, if one expresses the loop diagrams in terms of the tree-level matrix elements. The combination

$$r_{jk}^{q'}(p^2, m_{q'}, \mu) + J_{kj}, \quad j \leqslant 2 \quad \text{and} \quad k \geqslant 3, \quad (A2)$$

of the coefficients in Eq. (15) and the J_{kj}'s is scheme independent [28]. Substituting $r_{jk}^{q'}$ with Eq. (A2) in Eq. (33), one finds the scheme independent quantity:

$$\Delta\overline{\Gamma}_{\text{peng}} = \Delta\Gamma_{\text{peng}} + \frac{G_F^2 m_b^5}{64\pi^3} \times 2\,\text{Re}\left(-t\,\xi_u \xi_t^* \sum_{\substack{i,j=1,2 \\ k=3,\ldots,6}} C_i^{(0)} C_j^{(0)} J_{ki} b_{jk} + |\xi_t|^2 \sum_{\substack{i=1,2 \\ j,k=3,\ldots,6}} C_i^{(0)} C_j^{(0)} J_{ki} b_{jk} \right). \quad (A3)$$

Here $\xi_t^* = -\xi_u^* - \xi_c^*$ has been used. In the NDR scheme the J_{ki}'s in Eq. (A3) evaluate to [28]

$$J_{31} = -0.877, \quad J_{32}^{\text{NDR}} = -0.532,$$

$$J_{41} = 0.324, \quad J_{42}^{\text{NDR}} = -0.202,$$

$$J_{51}=0.557, \quad J_{52}^{\rm NDR}=0.511,$$

$$J_{61}=0.146, \quad J_{62}^{\rm NDR}=-0.677. \tag{A4}$$

The J_{k1}'s in the first row of Eq. (A4) do not depend on the renormalization scheme, because $r_{1j}^{q'}=0$ in all schemes due to a vanishing color factor.

In the same way one finds

$$\Delta\overline{\Gamma}_{cc}=t\,\frac{G_F^2 m_b^5}{64\pi^3}\,2|\xi_u|^2\sum_{i,j=1}^{2} C_i^{(0)}C_j^{(0)}\left(h_{ij}+\sum_{k=1}^{2} J_{ki}b_{kj}\right). \tag{A5}$$

Here the scheme dependence of the h_{ij}'s in Eq. (23) cancels with the one of the J_{ki}'s [28]:

$$J_{11}^{\rm NDR}=J_{22}^{\rm NDR}=\frac{631}{6348}=0.099, \quad J_{12}^{\rm NDR}=J_{21}^{\rm NDR}=\frac{3233}{2116}=1.528. \tag{A6}$$

If one inserts Eq. (A1) into $\Delta\Gamma_W$, one finds the J_{jk}'s with $k\leqslant 2$ to appear exactly in the combinations entering Eq. (A3) and Eq. (A5). The remaining J_{jk}'s with $k\geqslant 3$ describing penguin-penguin mixing would cancel the scheme dependence of the loop diagrams of Fig. 1 and Fig. 2 with insertions of penguin operators Q_j, $j=3,\ldots,6$. Since the latter are omitted in our calculation, we must also leave out the J_{jk}'s with $k\geqslant 3$ in Eq. (A1). This has been done in Table I. ΔC_j has been tabulated in the last line of Table I for illustration. It can be obtained from the other entries of the table with the help of Eqs. (A1), (A6), and (A4). Finally $\Delta\overline{\Gamma}_W$ is simply obtained from $\Delta\Gamma_W$ in Eq. (21) by replacing ΔC_j with $\Delta\overline{C}_j$.

Unlike $C_j^{(0)}$, $j\leqslant 6$, $C_8^{(0)}$ is a two-loop quantity and therefore *a priori* scheme dependent. We understand H in Eq. (12) to be renormalized such that the matrix elements $\langle dg|Q_j|b\rangle$ vanish at the one-loop level for $j=1,\ldots,6$. This ensures that $\Delta\Gamma_8$ as defined in Eq. (26) is scheme independent [27]. The thereby renormalized LO coefficient $C_8^{(0)}$ is usually called $\widetilde{C}_8$ or $C_8^{(0)\rm eff}$. In the NDR scheme this finite renormalization simply amounts to $C_8^{(0)}=C_8^{(0),\rm NDR}+C_5^{(0)}$. Apart from $\Delta\Gamma_8$ this only affects the penguin diagram of Q_5 (cf. Fig. 2), which is a part of the neglected radiative corrections to penguin operators.

[1] T. E. Browder, K. Honscheid, and D. Pedrini, Annual Review of Nuclear and Particle Science, Vol. 46 (1997), p. 395, hep-ph/9606354; T. E. Browder, in *ICHEP'96*, Proceedings of the 28th International Conference on High Energy Physics, Warsaw, Poland, edited by Z. Ajduk and A. Wroblewski (World Scientific, Singapore, 1997), p. 1139, hep-ph/9611373; J. D. Richman, *ibid.*, p. 143, hep-ex/9701014.

[2] CLEO Collaboration, B. Barish *et al.*, Phys. Rev. Lett. **76**, 1570 (1996); ARGUS Collaboration, H. Albrecht *et al.*, Phys. Lett. B **318**, 397 (1993).

[3] I. I. Bigi, N. Uraltsev, and A. Vainshtein, Phys. Lett. B **293**, 430 (1992); **297**, 477(E) (1993); B. Blok and M. Shifman, Nucl. Phys. **B399**, 441 (1993); **B399**, 459 (1993).

[4] A. Manohar and M. Wise, Phys. Rev. D **49**, 1310 (1994); B. Blok, L. Koyrakh, M. Shifman, and A. I. Vainshtein, *ibid.* **49**, 3356 (1994); **50**, 3572(E) (1994); T. Mannel, Nucl. Phys. **B413**, 396 (1994); I. I. Bigi, M. A. Shifman, N. G. Uraltsev, and A. I. Vainshtein, Int. J. Mod. Phys. A **9**, 2467 (1994).

[5] I. I. Bigi, B. Blok, M. Shifman, N. Uraltsev, and A. Vainshtein, in *B* decays, edited by S. Stone, 2nd ed. (World Scientific, Singapore, 1994), p. 132; I. I. Bigi, hep-ph/9508408.

[6] M. Neubert and C. Sachrajda, Nucl. Phys. **B483**, 339 (1997).

[7] I. J. Kroll, in *17th International Symposium on Lepton-Photon Interactions*, Proceedings, Beijing, China, 1995, edited by Z. Zheng and H. Chen (World Scientific, Singapore, 1996), hep-ex/9602005.

[8] E. Bagan, P. Ball, V. M. Braun, and P. Gosdzinsky, Nucl. Phys. **B432**, 3 (1994).

[9] E. Bagan, P. Ball, B. Fiol, and P. Gosdzinsky, Phys. Lett. B **351**, 546 (1995).

[10] E. Bagan, P. Ball, V. M. Braun, and P. Gosdzinsky, Phys. Lett. B **342**, 362 (1995); **374**, 363(E) (1996).

[11] G. Altarelli and S. Petrarca, Phys. Lett. B **261**, 303 (1991).

[12] M. Neubert, in the Proceedings of the 10th Les Rencontres de Physique de la Vallee d'Aoste, La Thuile, 1996 (unpublished), hep-ph/9605256.

[13] G. Buchalla, I. Dunietz, and H. Yamamoto, Phys. Lett. B **364**, 188 (1995).

[14] I. Dunietz, J. Incandela, F. D. Snider, and H. Yamamoto, hep-ph/9612421.

[15] ALEPH Collaboration, contribution to the International Europhysics Conference on High Energy Physics, Brussels, 1995 (unpublished), EPS-404; DELPHI Collaboration, P. Abreu *et al.*, Z. Phys. C **66**, 323 (1995); L3 Collaboration, M. Acciarri *et al.*, Z. Phys. C **71**, 379 (1996); OPAL Collaboration, R. Akers *et al.*, Z. Phys. C **60**, 199 (1993).

[16] M. Neubert, in the Proceedings of the 20th Johns Hopkins Workshop on Current Problems in Particle Theory, Heidelberg, 1996 (unpublished), hep-ph/9610385.

[17] S. Bertolini, F. Borzumati, and A. Masiero, Nucl. Phys. **B294**, 321 (1987); A. L. Kagan, Phys. Rev. D **51**, 6196 (1995); M. Ciuchini, E. Gabrielli, and G. F. Giudice, Phys. Lett. B **388**, 353 (1996); A. L. Kagan and J. Rathsman, hep-ph/9701300.

[18] W. F. Palmer and B. Stech, Phys. Rev. D **48**, 4174 (1993).

[19] R. Fleischer, Z. Phys. C **58**, 483 (1993).

[20] G. Altarelli, G. Curci, G. Martinelli, and S. Petrarca, Nucl. Phys. **B187**, 461 (1981).

[21] W. A. Bardeen, A. J. Buras, D. W. Duke, and T. Muta, Phys. Rev. D **18**, 3998 (1978).

[22] A. F. Falk, Z. Ligeti, M. Neubert, and Y. Nir, Phys. Lett. B **326**, 145 (1994).

[23] G. Buchalla, Nucl. Phys. **B391**, 501 (1993).

[24] A. J. Buras and R. Fleischer, Phys. Lett. B **341**, 379 (1995).

[25] M. Ciuchini, E. Franco, G. Martinelli, and L. Silvestrini, hep-ph/9703353.

[26] M. A. Shifman, A. I. Vainshtein, and V. I. Zakharov, Phys.

Rev. D **18**, 2583 (1978); *ibid.* **19**, 2815(E) (1979); B. Grinstein, R. Springer, and M. B. Wise, Phys. Lett. B **202**, 138 (1988); Nucl. Phys. **B339**, 269 (1990).

[27] M. Ciuchini, E. Franco, G. Martinelli, L. Reina, and L. Silvestrini, Phys. Lett. B **316**, 127 (1993); M. Ciuchini, E. Franco, L. Reina, and L. Silvestrini, Nucl. Phys. **B421**, 41 (1994); M. Ciuchini, E. Franco, G. Martinelli, L. Reina, and L. Silvestrini, Phys. Lett. B **334**, 137 (1994).

[28] A. J. Buras, M. Jamin, M. E. Lautenbacher, and P. H. Weisz, Nucl. Phys. **B370**, 69 (1992); Addendum *ibid.* **B375**, 501 (1992); A. J. Buras, M. Jamin, M. E. Lautenbacher, and P. H. Weisz, *ibid.* **B400**, 37 (1993).

[29] S. Bethke, in *QCD 96*, Proceedings of the Conference, Montpellier, France, 1996, edited by S. Narison [Nucl. Phys. B (Proc. Suppl.) **54A**, 314 (1997)], hep-ex/9609014.

[30] S. Herrlich and U. Nierste, Nucl. Phys. **B455**, 39 (1995); **B476**, 27 (1996).

[31] H. Simma, G. Eilam, and D. Wyler, Nucl. Phys. **B352**, 367 (1991).

[32] Y. Nir, Phys. Lett. B **221**, 184 (1989).

[33] I. Bigi, M. Shifman, and N. Uraltsev, hep-ph/9703290.

[34] M. Artuso, Nucl. Instrum. Methods Phys. Res. A **384**, 39 (1996).

[35] S. Herrlich and U. Nierste, Phys. Rev. D **52**, 6505 (1995); U. Nierste, in *Proceedings of the Workshop on K physics*, Orsay, France, 1996 edited by L. Iconomidou-Fayard (Editions Frontieres, Gif-Sur-Yvette, 1997) hep-ph/9609310.